

Modeling the Effects of UV Variability and the QBO on the Troposphere–Stratosphere System. Part I: The Middle Atmosphere

NAMBATH K. BALACHANDRAN

Global Systems Institute, Columbia University, New York, New York

DAVID RIND

Global Systems Institute, Columbia University, and NASA/Goddard Institute for Space Studies, New York, New York

(Manuscript received 23 June 1994, in final form 8 March 1995)

ABSTRACT

Results of experiments with a GCM involving changes in UV input ($\pm 25\%$, $\pm 10\%$, $\pm 5\%$ at wavelengths below $0.3 \mu\text{m}$) and simulated equatorial QBO are presented, with emphasis on the middle atmosphere response. The UV forcing employed is larger than observed during the last solar cycle and does not vary with wavelength, hence the relationship of these results to those from actual solar UV forcing should be treated with caution. The QBO alters the location of the zero wind line and the horizontal shear of the zonal wind in the low to middle stratosphere, while the UV change alters the magnitude of the polar jet and the vertical shear of the zonal wind. Both mechanisms thus affect planetary wave propagation. The east phase of the QBO leads to tropical cooling and high-latitude warming in the lower stratosphere, with opposite effects in the upper stratosphere. This quadrupole pattern is also seen in the observations. The high-latitude responses are due to altered planetary wave effects, while the model's tropical response in the upper stratosphere is due to gravity wave drag.

Increased UV forcing warms tropical latitudes in the middle atmosphere, resulting in stronger extratropical west winds, an effect which peaks in the upper stratosphere/lower mesosphere with the more extreme UV forcing but at lower altitudes and smaller wind variations with the more realistic forcing. The increased vertical gradient of the zonal wind leads to increased vertical propagation of planetary waves, altering energy convergences and temperatures. The exact altitudes affected depend upon the UV forcing applied.

Results with combined QBO and UV forcing show that in the Northern Hemisphere, polar warming for the east QBO is stronger when the UV input is reduced by 25% and 5% as increased wave propagation to high latitudes (east QBO effect) is prevented from then propagating vertically (reduced UV effect). The model results are thus in general agreement with observations associated with solar UV/QBO variations, although the west phase is not absolutely warmer with increased UV. Questions remain concerning the actual variation of stratospheric winds with the solar cycle as the magnitude of the variations reported in some observations cannot be associated with UV variations in this model (but do arise in the model without any external forcing). The model results actually come closer to reproducing observations with the reduced magnitude of UV forcing due to the lower altitude of west wind response, despite the smaller wind variations involved. An evaluation of the reality of the reported effects of combined QBO and solar UV variations on the middle atmosphere requires the use of proper UV solar cycle forcing and should include possible ozone variations.

1. Introduction

It has been suggested by the results from a number of studies (Holton and Tan 1980, 1982; Labitzke 1982; van Loon and Labitzke 1987) that the quasi-biennial oscillation (QBO), while primarily an equatorial phenomenon, may affect various processes at higher latitudes, especially in the polar regions. Holton and Tan (1980, 1982) showed that polar regions were warmer during the east phase of the QBO, with increased geopotential heights, while low latitudes had reduced temperatures and heights. Labitzke (1982) pointed out that stratospheric warmings are more likely during the east

phase of the QBO than during the west phase. Dunkerton et al. (1988) also reported a connection between QBO and major stratospheric warmings and stated that nonoccurrence of the major warmings is associated with deep equatorial westerlies. Dameris and Ebel (1990), using a model with perpetual lower-boundary forcing of long waves for wavenumbers 1 and 2, found that the simulated stratospheric warming, even though present during both east and west phases of the QBO, is enhanced during the east phase. Balachandran et al. (1991) has also reported experiments with the use of a GCM, which showed that stratospheric warmings are strengthened during the east phase of the QBO and weakened during the west phase. Thus, the impact of lower-stratosphere tropical zonal wind changes on extratropical stratospheric

Corresponding author address: Dr. David Rind, NASA/GISS, 2880 Broadway, New York, NY 10025.

processes has been found in both observational and modeling studies.

The effect of solar variability on weather and climate has been a controversial subject for a long time. In the most recent resurgence of research, Labitzke (1987) and van Loon and Labitzke (1988) published results showing significant correlation between the flux of the 10.7-cm solar radiation and geopotential heights of the 50-mb pressure surface when the data are grouped by the west and east phases of the QBO. In a refinement of their earlier findings, Labitzke and van Loon (1992) (Labitzke–van Loon studies will hereafter often be referred to as LvL) report that the north polar region is warmer during the east phase of the QBO than during the west phase (in a statistically significant way) only during the solar minima and that the region is warmer in the west phase than in the east phase during solar maxima. Dunkerton and Baldwin (1992) showed that this last result is prevalent in the region surrounding 100 mb only during February. These statistical results thus show an apparent modulation of the QBO effects by solar variations during at least some months, or, equivalently, a modulation of the solar effects on the atmosphere by the QBO. The problem is to find the physical mechanism of such modulation, if one actually exists.

The Labitzke and van Loon correlations extend from the middle atmosphere down into the troposphere. Given the much greater mass and energy of the lower levels, the relatively small variation in total energy associated with solar variability (on the order of 0.1% during the last solar cycle), and the lack of obvious physical coupling mechanisms, the results have been treated with some skepticism. For example, Salby and Shea (1991) suggest that the solar–atmospheric correlations may be explained by statistical considerations related to sampling and the lengths of record available for correlation, although Kodera (1993) argues that the results are maintained in an analysis that does not decrease the sampling frequency of the original signal. Overall, the Labitzke and van Loon correlations have passed relatively stringent significance tests and have been considered sufficiently useful to be incorporated in techniques for the seasonal forecasting of the United States weather (Barnston and Livezey 1989).

Kodera et al. (1990) have used a general circulation model to show that perturbations to winds in the upper stratosphere associated with ozone heating rates of –30% to +20% (equivalent to UV variations of that magnitude) can propagate to lower levels, a result apparently consistent with observations (Kodera 1991). The altered ultraviolet radiation will primarily affect ozone-rich regions receiving appreciable solar insolation (i.e., lower latitudes in the upper stratosphere), changing the thermal gradients and thus wind fields. In that sense, both solar variability and the QBO are associated with zonal wind perturbations, which may

then affect wave propagation and wave–mean flow interactions.

Our objective in the following studies is to conduct experiments with a GCM in order to shed some light on the possible mechanism or mechanisms of such solar cycle and QBO effects on the troposphere–stratosphere system. The UV variations employed are larger than has been observed during the last solar cycle and do not vary with wavelength; thus, the conclusions from these experiments cannot directly prove or disprove the reported solar UV effects. Nevertheless, they do suggest pathways in which solar forcing could operate if the system is sufficiently sensitive. The results are reported in two phases: the model's middle atmosphere response to ultraviolet and QBO perturbations (Part I) and then the tropospheric response (Part II).

2. Model

The model used for the experiments is the Goddard Institute for Space Studies (GISS) Global Climate Middle Atmosphere Model (Rind et al. 1988a,b). The model has a resolution of $8^\circ \times 10^\circ$ (lat \times long), extends from the surface to 85 km, and includes a full array of processes: numerical solution of the primitive equations, radiative and surface fluxes, complete hydrological cycle, convective and cloud cover parameterizations, etc. as in the GISS climate model (Hansen et al. 1983). In addition, the model incorporates a simple parameterization for gravity wave drag (Rind et al. 1988a). Gravity wave effects due to topography, wind shear, and convection are calculated at each grid box from model-generated temperature and wind fields, and linear saturation theory is employed to determine levels of wave breaking. The model was run for 10 years and, with the aid of the gravity wave parameterizations, produced a realistic simulation with a proper break between tropospheric and stratospheric jets, realistic closing off of the winter time jet in the mesosphere, warm winter and cold summer polar mesospheric temperatures, stratospheric warmings of different degrees, etc. (Rind et al. 1988a,b). The primary deficiencies of the model are somewhat reduced long-wave energy in the troposphere and lower stratosphere, too cold temperatures near the model top, and too warm temperatures in the Southern Hemisphere polar lower stratosphere.

3. Experiments

The basic aim of the experiments is to determine what effects the changes in UV radiation and the QBO have on the troposphere–stratosphere system. Since the largest percentage variability in the incoming solar radiation occurs in wavelengths shorter than the visible (e.g., Lean 1991), our experiments involve solar radiation changes in the model at wavelengths less than $0.3 \mu\text{m}$. The solar UV input below $0.3 \mu\text{m}$ was altered

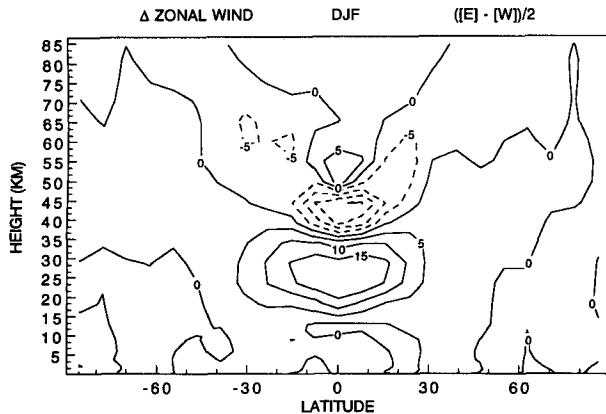


FIG. 1. Three-year composite annual average wind difference between W QBO and E QBO (W minus E) divided by 2 showing the equatorial west wind forcing between 20-km and 40-km altitudes in the model. The easterlies and westerlies above are model generated by gravity wave drag and E-P flux divergence.

with reference to the normal values in the control run by $\pm 25\%$, $\pm 10\%$, and $\pm 5\%$. The actual solar ultraviolet radiation changes are still somewhat uncertain, although current estimates, from considering the variations that occur associated with solar rotation and from *UARS* measurements, are for changes of about 8% at $0.2 \mu\text{m}$, 4% by $0.25 \mu\text{m}$, and less than 1% at $0.3 \mu\text{m}$ (Lean et al. 1992; J. Lean 1995, personal communication). Thus, all these experiments use variations larger than the observed, especially for wavelengths near $0.3 \mu\text{m}$, although the $\pm 5\%$ runs are much closer to reality. The values at wavelengths less than $0.2 \mu\text{m}$ are actually underestimated in the less extreme UV experiments; this will primarily affect regions above the stratopause. Variations at wavelengths longer than $0.3 \mu\text{m}$ may account for some 80% of the total irradiance variations (Lean 1991) and are not included in these experiments; such effects would be felt primarily in the troposphere. The approach is thus to provide an exaggerated forcing with the UV radiation input so as to discern any gross impacts in the middle atmosphere and potential coupling into the lower atmosphere; the gross aspect of these experiments is similar to that of Kodera et al. (1990), although at the $\pm 5\%$ level they are closer to reality than has heretofore been employed. Nevertheless, given the still exaggerated nature of the forcing, the results of these experiments cannot literally be related to actual solar UV forcing. Future experiments should use best estimates of solar variability at different wavelengths.

We also did not alter the atmospheric ozone distribution from the control run, even though stratospheric ozone in the real atmosphere may change with the solar cycle (e.g., Hood et al. 1993). Future experiments should incorporate realistic changes in ozone, which will again alter the level and magnitude of absorbed radiation somewhat.

Since the studies referred to earlier point to the modulation of the solar effects by the equatorial QBO (or the reverse), we also conducted experiments with a simulated QBO in the Tropics. The model by itself does not generate the QBO, probably due to lack of sufficient resolution. To simulate the QBO, the equatorial winds at the 31.6-mb and 14.7-mb levels in the model were forced to -25 m s^{-1} for the case of east QBO and $+25 \text{ m s}^{-1}$ for the west case with a time constant of 30 days, employing an exponential falloff away from these levels and from the equator. In effect, the forcing extends to 27°N,S . (We did, however, run a few cases with forcing extending only up to 8°N,S .) A comparison of the resulting wind differences between, for example, the west QBO and the east QBO (divided by 2) is presented in Fig. 1. The resultant effect, a combination of the forcing and the model response, is in good agreement with the actual phenomenon (e.g., Fig. 8.2 of Andrews et al. 1987) in terms of the vertical and latitudinal distribution of wind amplitudes. However, the model forcing is obviously not generated in the same manner as the observed; what difference this makes in the results is not known. Also uncertain is the impact of using a steady forcing of the peak winds of the QBO rather than simulating the transitional phenomena. We are essentially experimenting with the gross effects of strong east and west winds in the tropical lower stratosphere (the tropical region mainly affected by the QBO).

The various UV and QBO runs were each done separately and then in combination. A list of the model experiments discussed in these papers is presented in Table 1, along with the number of years of integration. The results given below will, in general, be averages for three years of the experiments; however, to increase

TABLE 1. Characteristics of the model runs.

| Model | UV radiation | OBO forcing | Number of years run |
|---------|--------------|-------------|---------------------|
| Control | Normal | None | 10 |
| +25 | +25% | None | 3 |
| -25 | -25% | None | 3 |
| W | Normal | West | 3 |
| E | Normal | East | 3 |
| +25W | +25% | West | 3 |
| +25E | +25% | East | 3 |
| -25W | -25% | West | 3 |
| -25E | -25% | East | 3 |
| +10W | +10% | West | 10 |
| +10E | +10% | East | 10 |
| -10W | -10% | West | 10 |
| -10E | -10% | East | 10 |
| +10 | +10% | None | 3 |
| -10 | -10% | None | 3 |
| +5W | +5% | West | 3, 10 |
| +5E | +5% | East | 3, 10 |
| -5W | -5% | West | 3, 10 |
| -5E | -5% | East | 3, 10 |
| +5 | +5% | None | 3, 10 |
| -5 | -5% | None | 3, 10 |

the statistical significance and stability of the model results, the 5% UV variations experiments were all extended to 10 years. It will be shown that the 10-year averages are almost identical to the 3-year results. All model runs followed a spinup of several months, which proved sufficient given that the sea surface temperatures were not allowed to change. The focus of this paper and Part II will be on the "wider" QBO in combination with the more extreme UV forcing and then with the most realistic solar forcing to illustrate the mechanisms involved. The effects of the intermediate UV forcing ($\pm 10\%$) and the more narrow QBO forcing (not listed in the table) will be introduced primarily to investigate the model sensitivity to changes in forcing.

A note on the "significance" of the results: in both the middle atmosphere and the troposphere, changes are generally on the order of one standard deviation of the model's normal interannual variation (which is often true for the observations as well). Therefore, to evaluate the "reality" of the effect in the model, we initially relied upon the similarity of physical interpretations derived from model output across the suite of experiments. Subsequently, results were checked with the 10-year experiments, which provided an indication of their strong consistency and did produce areas of statistically significant results. Where consistency does occur, this check implies statistical significance would be increased by integrating the experiments for a much longer time.

4. QBO results

a. The QBO wind response with different UV forcing

Before discussing specific results from the model and relating them to the observational studies referred to earlier, it is instructive to examine the overall general pattern of atmospheric circulation changes brought about by variations in the incoming UV radiation and the tropical QBO. Since the QBO-modulated solar effects are mainly reported to be observed in the winter circulation and hence there is a strong possibility that the coupling may be through planetary waves, we will concentrate on the changes in the northern winter middle atmosphere jet and the zero-wind line separating the westerlies from the easterlies in the two hemispheres, both of which are characteristics that may alter planetary wave propagation conditions.

The impact of the different forcing on these two features is summarized in Table 2, while the model-generated winds are shown for the control run, the two pure QBO experiments [E] and [W], and the two extreme UV change only experiments, [+25] and [-25], in Fig. 2. In the west phase of the QBO the results, almost independent of UV forcing, show the zero wind line in the Southern Hemisphere up to 35 km, and in the Northern Hemisphere above to at least 50 km. In the east phase, the zero wind line falls in the Northern Hemisphere up to at least 60 km. The control run is

more like the east phase QBO in the position of its zero wind line. Note that the tropical wind response without *any* UV variations (i.e., runs [E] and [W]) is basically the same as with the UV variations, both positive and negative.

The QBO has a discernible impact on the strength of the peak stratospheric jet, averaging 8 m s^{-1} more during the east phase, regardless of the UV variation. There is also an influence on the latitude of the peak stratosphere jet: in [W] it is further poleward than in [E]. This also holds true to some extent when the solar forcing is involved, more often with UV reductions. An obvious connection between the effect of the QBO and UV forcing on both the zero wind line and the winter jet involves wave-energy propagation, as will be discussed below.

In Fig. 3 is presented the change of the zonal wind between the east and west phases of the QBO for the extreme UV maxima and minima (left-hand side) and the more realistic UV variations (right-hand side). (For the picture with no UV variations, refer to Fig. 1 and multiply the values by 2.) In addition to the expected tropical lower stratospheric change, the outstanding feature is a change of the opposite sign in the upper stratosphere in each experiment. This is the result of momentum forcing, here the product of the parameterized convective gravity wave drag and to a lesser extent the Eliasson-Palm (E-P) flux divergence due to planetary waves, providing increased west wind acceleration for the E phase and increased east wind acceleration for the W phase. The convective gravity waves are parameterized in the model with both positive and negative phase speeds (Rind et al. 1988a). With east winds in the lower stratosphere, the slower westward traveling waves cannot propagate upward, while the eastward modes reach the middle and upper stratosphere. There they break, with their drag decelerating the east winds. The opposite conditions exist for the W phase; the westward traveling convectively generated gravity waves break in the middle and upper stratosphere leading to the acceleration of easterlies there.

In Fig. 4 is shown the difference in wind forcing due to gravity wave drag (top) and the E-P flux divergence (bottom) for [+25E minus +25W]. The upper-stratospheric tropical warming is caused by the acceleration of the west wind component by a combination of gravity wave drag and E-P flux divergence. Similar results follow for the -25E minus -25W case.

To verify the effects of gravity waves on the structure of the tropical wind response, we eliminated the parameterized convective gravity waves in the model. The east minus west plots showed that while the lower-stratospheric temperature and wind pattern indicated little change, the upper-stratospheric wind pattern changed significantly. The center of the west wind region moved upward into the mesosphere, the west acceleration now being provided mainly by E-P flux di-

TABLE 2. Characteristics of middle atmosphere jet and zero wind line for northern winter (composite average for Dec–Jan–Feb).

| Model | Latitude (°N) | Altitude (km) | Core speed (m s ⁻¹) | Zero wind line* |
|---------|------------------|------------------|------------------------------------|--|
| Control | 63 | 55 | 77 | NH up to 50 km, SH above |
| +25 | 63 | 55 | 89 | NH up to 50 km, SH above |
| -25 | 55 | 55 | 68 | NH up to 50 km, SH above |
| W | 63 | 55 | 74 | SH up to 35 km, NH to 50 km, SH above |
| E | 55 | 55 | 79 | Entirely in the NH |
| +25W | 55 | 55 | 78 | SH up to 35 km, NH to 50 km, SH above |
| +25E | 55 | 55 | 89 | NH up to 60 km, SH above |
| -25W | 55 | 55 | 60 | SH up to 35 km, NH above |
| -25E | 55 | 55 | 71 | Entirely in the NH |
| +10 | 55 | 55 | 83 | NH up to 50 km, SH above |
| -10 | 63 | 55 | 69 | NH up to 50 km, SH above |
| +10W | 63 | 55 | 78 | SH up to 35 km, NH to 50 km, SH above |
| +10E | 55 | 55 | 89 | Entirely in the NH |
| -10W | 63 | 50 | 66 | SH up to 35 km, NH above |
| -10E | 55 | 55 | 74 | Entirely in the NH |
| +5 | 55 | 55 | 76 | NH up to 50 km, SH above |
| -5 | 63 | 55 | 81 | NH up to 50 km, SH above |
| +5W | 55 | 55 | 75 | SH up to 35 km, NH to 50 km, SH above |
| +5E | 55 | 55 | 80 | NH up to 60 km, SH above |
| -5W | 63 | 50 | 68 | SH up to 35 km, NH up to 50 km, SH above |
| -5E | 55 | 55 | 79 | NH up to 60 km, SH above |

* Individual levels can be different from the general description.

vergence. We will show later that the [E – W] observational data verify the location of the warm anomaly region occurring in the equatorial upper stratosphere. Therefore, the model is most successful in simulating observations when using the parameterization for a broad phase velocity spectrum of convective gravity waves.

The extratropical response to the east phase of the QBO indicates a small weakening of stratospheric west winds (note the extension of the zero wind change contour in Fig. 3 toward higher latitudes in all four experiments). Plumb (1984) noted that the increased polar temperatures in the lower stratosphere during the east phase of the QBO (compared to the west phase) should lead to the reduction of the high-latitude west wind jet by about 5 m s⁻¹, which is consistent with the result in most of these experiments. However, with -5% UV the reduction is substantially greater.

b. The QBO temperature response with different UV forcing

In Fig. 5 is shown the 3-year composite average temperature difference between east and west QBO runs [E minus W] and with different UV forcings. A cold region (of -4° to -6°C) brought about by the QBO forcing is present in the equatorial region centered around 20-km altitude. The QBO also induces a warm region above the cold region with similar magnitude. The tropical lower stratospheric cooling is directly associated with the QBO forcing employed; an east wind circulation requires a reverse latitudinal temperature

gradient, with warming in the subtropics and cooling in the Tropics. This is accomplished by a mean circulation change with greater rising air in the tropical lower stratosphere (e.g., Andrews et al. 1987).

The warming directly above, in the tropical middle and upper stratosphere, is also due to a circulation change. Given that the gravity wave drag is responsible for the change in sign of the wind anomaly in this region, it is also responsible for the warming here, as the increased latitudinal temperature gradient is consistent with a west wind anomaly from the thermal wind relationship. The effect is accomplished in the model through relative subsidence in the Tropics at these levels.

In the extratropics, the east wind phase is associated with warmer conditions in the high latitude winter lower stratosphere. The warming is slightly greater with reduced UV in the 25% experiments, but it is much greater with reduced UV in the 5% experiments. In both the reduced UV experiments, the warming is centered over the polar regions, in contrast to the effect with increased UV, when the warming maximizes at midlatitudes. These results are consistent with the observations of LvL except that no absolute polar cooling is found with increased UV. A region of cooling of somewhat greater intensity overlays the warm region. Additional warm and cold regions in the mesosphere extend into the summer hemisphere. The basic pattern appears in all the experiments.

This result of tropical/extratropical lower stratospheric cooling/warming overlain by warming/cooling forms a quadrupole structure of the temperature pat-

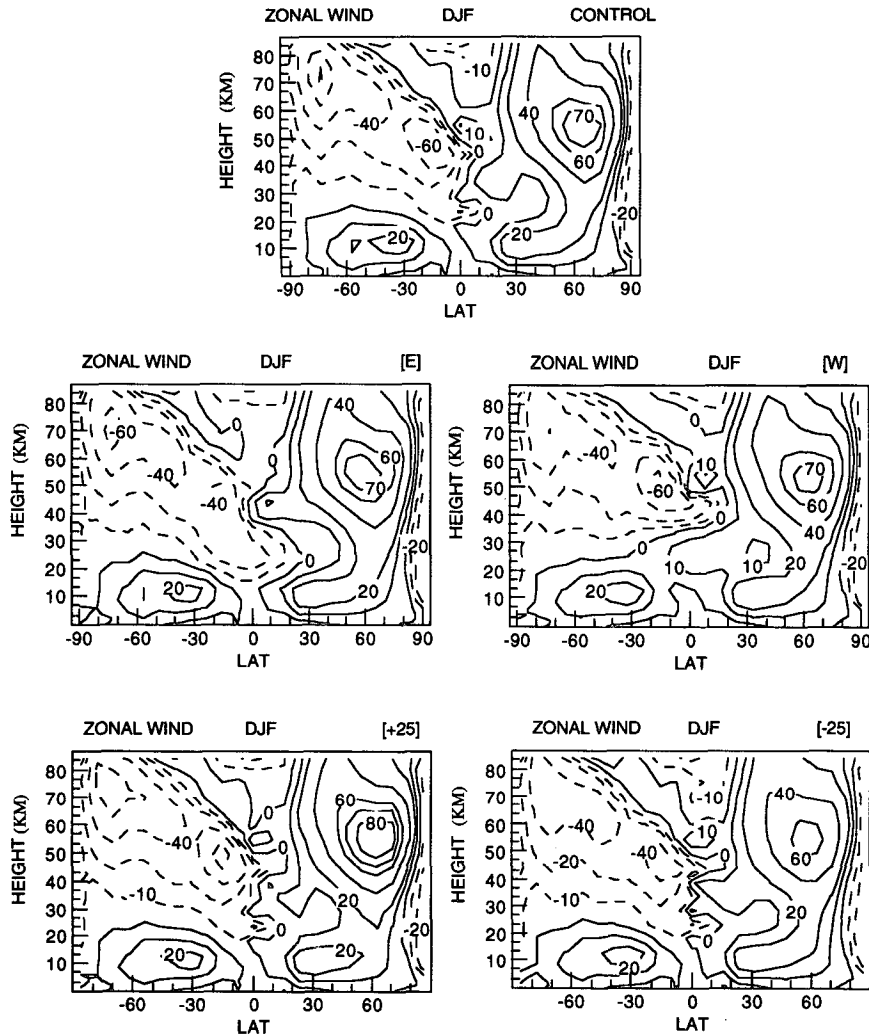


FIG. 2. Three-year composite average zonal wind for northern winter (Dec–Jan–Feb) for the control run (top); [E] (middle left); [W] (middle right); [+25] (bottom left); [–25] (bottom right).

tern in the winter hemisphere. The quadrupole pattern is not as pronounced in the summer hemisphere but is present in both hemispheres in the model runs during their respective winters and for all UV changes. It is, however, absent in the experiments with a QBO forcing confined to 8°N,S , as the high-latitude response is largely missing. The ability of the QBO to affect the extratropics in this model appears to be a function of the width of the equatorial forcing. The influence of the width of the equatorial QBO on the extratropical QBO has also been reported by O’Sullivan and Dunkerton (1994).

To compare the model results with observations, we analyzed 12 years of National Meteorological Center (NMC) temperature data. Shown in Fig. 6 are the plots of temperature differences (E QBO minus W QBO) for northern winter (top) and southern spring (bottom) for the NMC data. The quadrupole pattern in each

hemisphere of lower stratospheric extratropical warming with the cooling above and the reversed pattern in the Tropics is clearly visible, being stronger in northern winter and weaker in southern spring, a result which is also present in the model. Even the weaker quadrupole effect in the summer hemisphere is evident. That both the model and observational data show these patterns is probably a testimony to the dominance of planetary wave propagation effects associated with tropical zonal wind variations; the contribution of altered planetary wave fluxes to extratropical temperature changes in observed data has been analyzed by Dunkerton and Baldwin (1991). It is also to some extent a verification of the effects of tropical zonal winds on gravity wave propagation, which are thought to generate the QBO itself.

Holton and Tan (1982) showed that the geopotential height differences in the lower stratosphere at

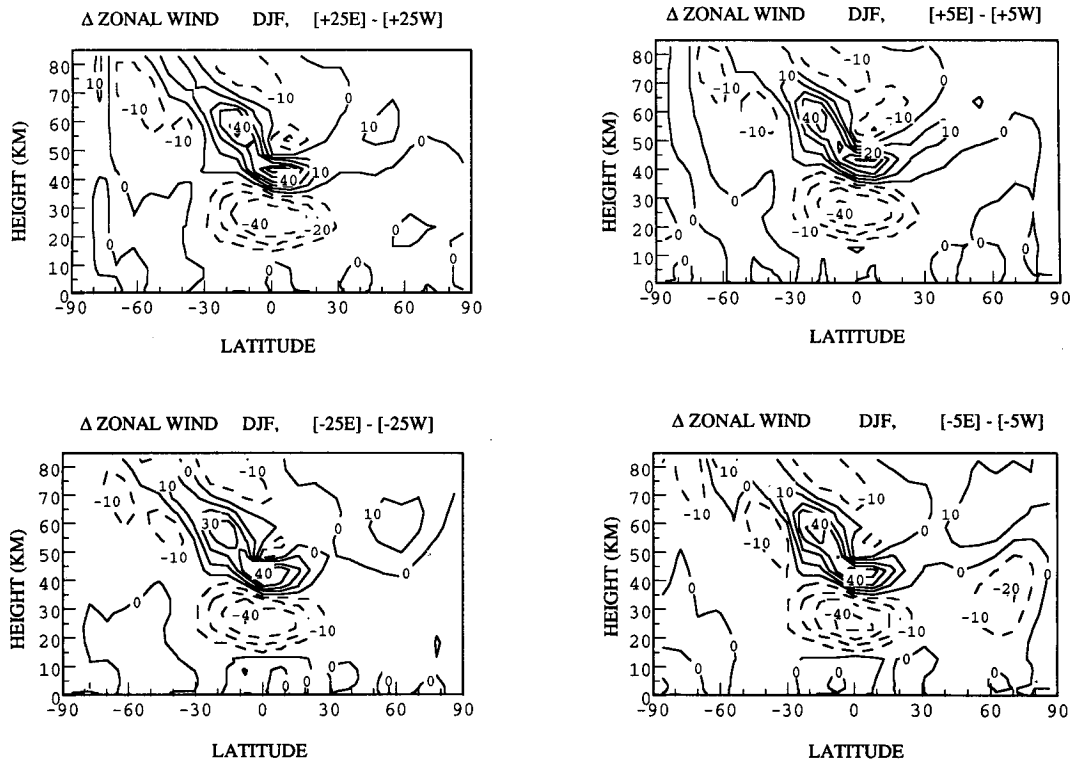


FIG. 3. Zonal wind changes for QBO experiments (composite averages for Dec–Feb): [+25E] minus [+25W] (top left); [−25E] minus [−25W] (bottom left); [+5E] minus [+5W] (top right); [−5E] minus [−5W] (bottom right). Contour intervals: 10 m s^{−1}.

high latitudes were negative for the west phase of the QBO compared with the east phase, and positive in the Tropics. The results of our experiments are consistent with those observations (which did not differentiate between the phase of the solar cycle), a direct response to the temperature changes in the lower stratosphere. In Fig. 7 (left) is presented the height differences for [−5W minus −5E] and in Fig. 7 (right), the same plot for [+5W minus +5E]. In both diagrams the height differences are negative at high latitudes and positive at low latitudes, in agreement with the analysis of observational data; the same is true for the experiments with no UV forcing [E − W] (not shown). The magnitudes of change are also consistent with the reported values. The height differences are larger in the reduced UV run as indicated by LvL and are actually close to zero near the pole with increased UV; however, again, the increased UV results do not indicate *positive* height differences at high latitudes. Dunkerton and Baldwin (1992) noted that the positive values referred to by LvL for solar minima exist only for specific winter months (i.e., February); however, a search of the model results failed to indicate any significant monthly differences that contrast with the seasonal picture shown here.

c. Explanation of QBO response

What accounts for the pattern in the model and the differences associated with altered UV? The temperature differences are all due to dynamical processes since they appear with no change in UV irradiances but differing QBO phases; shortwave radiative changes arise from cloud cover changes in the upper troposphere, but the magnitudes are small [$O(0.1^{\circ}\text{C day}^{-1})$] compared to the dynamical changes of $O(1\text{--}10^{\circ}\text{C day}^{-1})$.

The extratropical temperature changes in the middle atmosphere are due primarily to altered wave propagation and energy convergence. The high-latitude lower stratospheric warming and upper-stratospheric cooling seen in Fig. 5 are associated with the change in E–P flux convergence and divergence, whose patterns of change are shown in Fig. 8. Relative poleward energy fluxes, E–P flux convergences, zonal wind decelerations, and extratropical warming occur in the Northern Hemisphere upper troposphere and lower stratosphere.

The change in E–P flux can be related to the wind changes presented in Fig. 3. The obvious difference between the E and W QBO (with all the UV forcings) is that up to 35 km in the middle atmosphere Tropics, the E runs have east winds, while the W runs have west winds. The east winds prevent the wave energy from propagating equatorward and vertically, and the waves

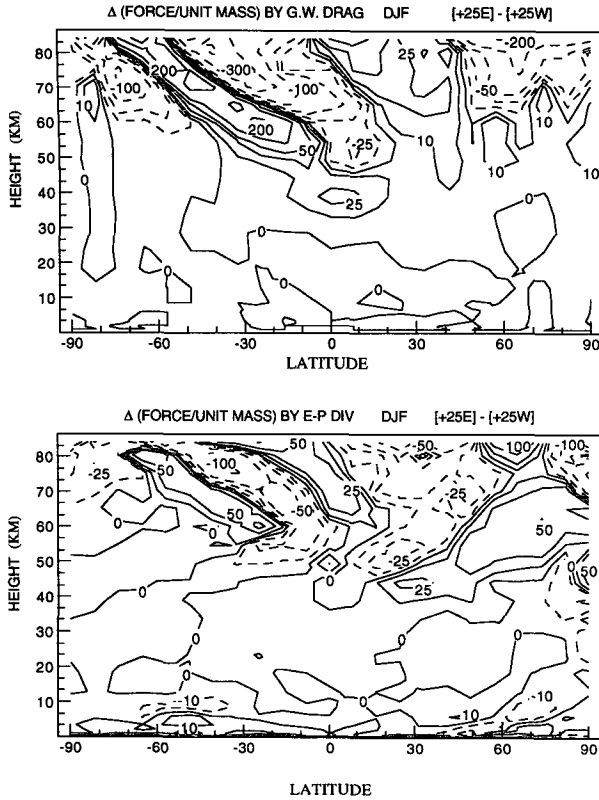


FIG. 4. Difference in force per unit mass for [+25E minus +25W] due to (top) gravity wave drag and (bottom) E-P flux divergence. Units 10^{-6} m s^{-2} .

refract poleward at these altitudes. At higher levels (above 35 km) in the Tropics the winds are greater west in the E runs (due to the gravity wave forcing mentioned previously), and relative equatorward refraction arises in the Northern Hemisphere. The E-P flux divergence contributes somewhat to the west acceleration at these levels as indicated in Fig. 4 (bottom).

The zonal mean quasigeostrophic refractive index for the vertical propagation of stationary planetary waves can be written

$$n^2 = N^2 f^{-2} [\partial q / \partial y (U - c)^{-1} - k^2 - (4H^2)^{-1}], \quad (1)$$

where N is the Brunt-Väisälä frequency, q the quasigeostrophic potential vorticity,

$$\partial q / \partial y = -\partial^2 U / \partial y^2 + \beta - e^{z/H} \partial (f^2 e^{-z/H} N^{-2} \partial U / \partial z) / \partial z, \quad (2)$$

U the zonal mean wind, $\beta = \partial f / \partial y$, k the zonal wavenumber, and H the atmospheric scale height; all quantities represent zonal mean values. Shown in Table 3 for several of the different QBO experiments are the respective changes in the northward E-P fluxes, the first term in the refractive index formulation ($\partial q / \partial y$) and the full refractive index change (basically domi-

nated by the change in $\partial q / \partial y$ normalized by the change in the zonal wind) for the lower stratosphere. The use of quasigeostrophic diagnostics in a primitive equation model introduces significant errors. Nevertheless, the increase in $\partial q / \partial y$, a positive refraction index change, and greater northward wave energy propagation occur in all the QBO experiments in the low to middle stratosphere. The increase in $\partial q / \partial y$ occurs because stronger horizontal wind shears are occurring at lower midlatitudes than at upper midlatitudes due to the QBO influence, and there is some change in the vertical shear of the zonal wind. The more positive refraction index implies better vertical propagation conditions, and midlatitude wave energy, which in the control run refracted horizontally to lower latitudes, is now propagating vertically. Therefore, there is a *net loss* of southward E-P flux; hence a *gain* in northward E-P flux, greater E-P flux convergence at higher latitudes, and warming.

Above the extratropical region of warming in the [E - W] runs, there is a region of cooling (from about 30 to 60 km, Fig. 5). The E-P flux diagrams show relative divergence in the extratropics at these altitudes. In the control run, energy propagates vertically from about 30° to 70°N, while refracting southward at latitudes equatorward of 65°N, in conjunction with the refraction characteristics of the atmosphere [65°N is the mean position of the middle atmosphere jet in the model, and the change of quasigeostrophic potential vorticity (QGPV) with latitude maximizes there]. In the E runs, the polar warming in the lower stratosphere leads to decreased zonal winds in the middle stratosphere at midlatitudes (via the thermal wind relationship). This has the effect of reducing the QGPV gradient, limiting vertical propagation, and enhancing equatorward wave energy flux in the upper stratosphere (Fig. 8) with subtropical warming and extratropical cooling (Fig. 5).

The extratropical temperature and wind response are exaggerated with reduced UV, especially in the 5% experiments, an effect which can also be seen in the E-P flux vectors. A positive feedback results as the warmer polar conditions help generate an east wind anomaly, which then leads to more poleward energy propagation. The combined impact of QBO and UV wind alterations will be discussed following the section on solar forcing results.

5. UV variation results

a. The stratospheric temperature response to the magnitudes of UV forcing

Increased UV radiation is absorbed by ozone in the summer hemisphere and tropical regions, an effect which is absent in the noninsolated winter polar region. The temperature response with the extreme UV and more realistic UV experiments, with and without the QBO, is shown in Fig. 9. The magnitude of the summer

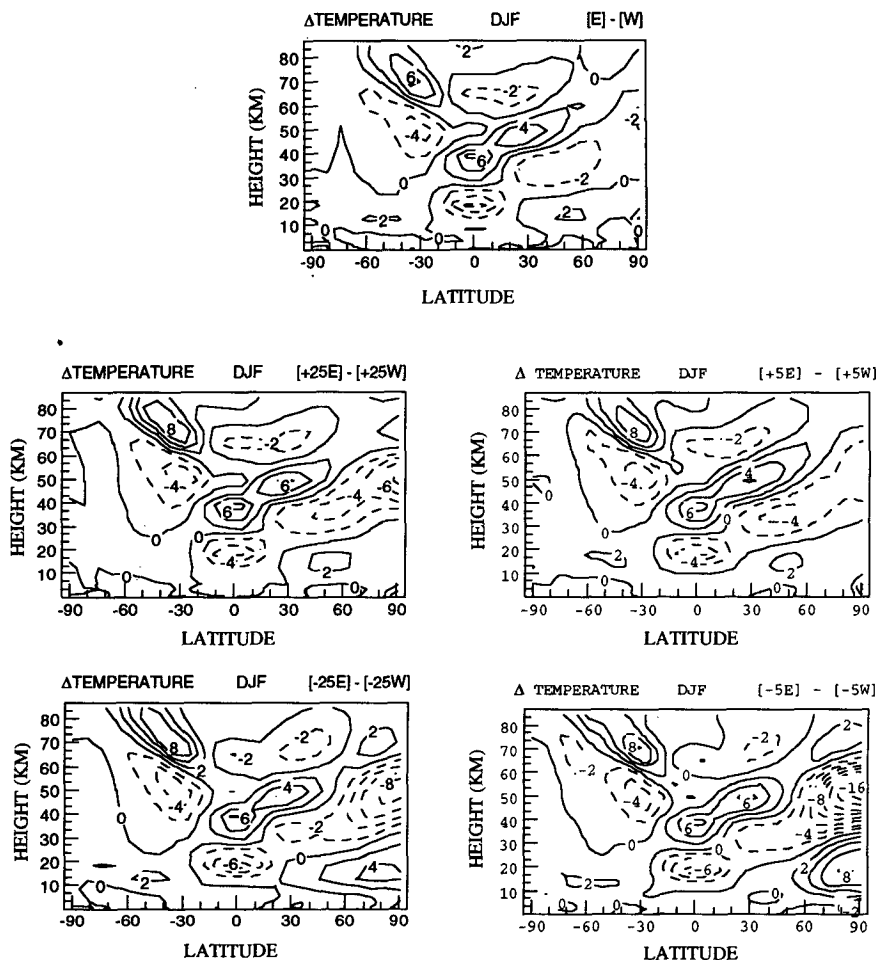


FIG. 5. Temperature differences for QBO experiments (composite averages for Dec–Feb): [E minus W] (top); [+25E minus +25W] (middle left); [−25E minus −25W] (bottom left); [+5E minus +5W] (top right); [−5E minus −5W] (bottom right). Contour intervals, 2°C.

stratospheric heating is directly proportional to the UV change, but in the winter hemisphere substantial differences arise between the east and west phases of the QBO. During the east phase, the UV maximum has *colder* temperatures in the winter polar lower stratosphere, while during the west phase the UV maximum has relatively less cooling and, in the case of the more realistic UV variations, the west phase has absolutely *warmer* temperatures. The cooling of the polar lower stratosphere during the east phase and the warming during the west phase with UV maximum compared to UV minimum is in complete agreement with the LvL results, which indicated stratospheric warmings were more prevalent during the west phase at solar maximum and during the east phase at solar minimum.

b. The stratospheric wind response to the magnitudes of UV forcing

The temperature changes shown in Fig. 9 are associated with zonal wind variations. These are shown in

Fig. 10, and the extratropical changes are tabulated in Table 4a for the different UV extremes. With increased UV, the larger latitudinal temperature gradient in the 25% runs leads to substantial increases in the middle atmosphere zonal jet (see also Fig. 2, Table 2). As the UV forcing differential is reduced, the magnitude of the zonal wind velocity change becomes smaller and may even change sign; in particular, with $\pm 5\%$ UV variations, the west wind changes are small. This result is in some qualitative agreement with results from 2D models (e.g., Huang and Brasseur 1993) but in apparent disagreement with several sets of observations. Note that the UV variations have no effect on the location of the tropical zero wind line (Table 2).

Kodera and Yamazaki (1990) found an apparent correlation between the zonal winds in December at 1 mb and the solar sunspot number, with wind variations between solar maximum and minimum of some 50 m s^{-1} . In this GCM, not even the $\pm 25\%$ UV variations could produce that high an effect.

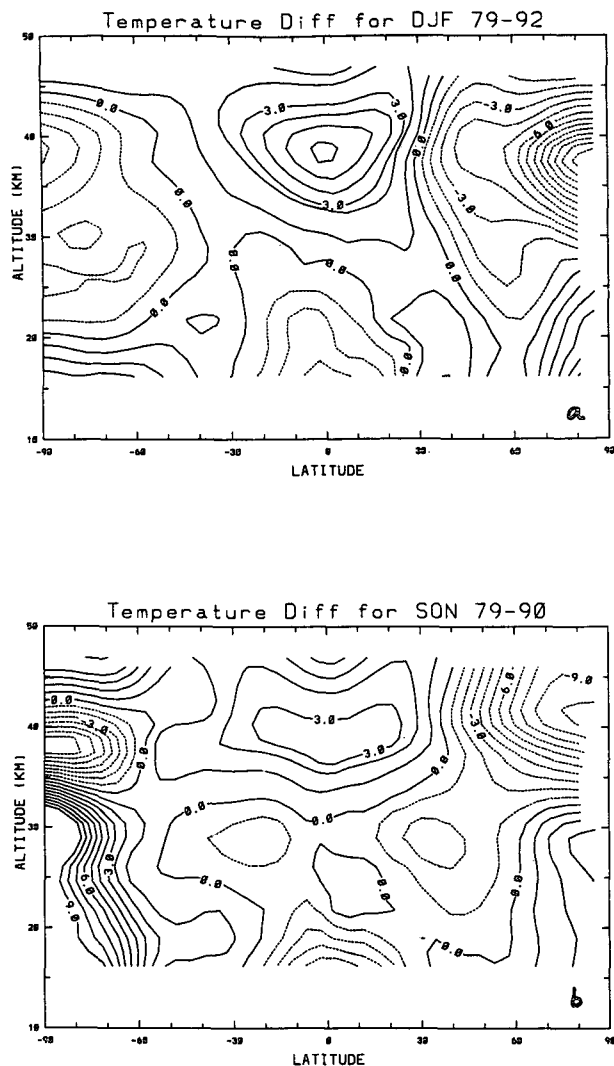


FIG. 6. Observed temperature differences (E QBO minus W QBO) for selected cases from the NMC data for (top) northern winter and (bottom) southern spring. Contour intervals, 1°C.

As only one seasonal cycle was involved in that observation, it is not at all apparent that variations of such magnitude are actually solar cycle connected. To illustrate this point, we present in Fig. 11 (top) the wind variations shown by Kodera and Yamazaki (1990) for 10 years (1976–85, hence solar minimum to solar minimum) and the variations of the model wind (Fig. 11, bottom) near its stratosphere jet from the control run, which was integrated for 10 years without any change in QBO phase or solar UV. The variations are obviously of the same order of magnitude; as discussed in Rind et al. (1988b), the model interannual standard deviations in the extratropics are in good agreement with observations. The similarity of the fluctuations shown in Fig. 11 does not mean that the observed winds are not solar cycle related, only

that caution needs to be exercised in arriving at that conclusion from one solar cycle in a system that (at least in the model) has similar magnitudes of natural variation.

Hood et al. (1993) repeated the correlation between solar UV and stratospheric winds using *Nimbus-7* Solar Backscatter Ultraviolet data with a gradient wind approximation and NMC data. They found a more modest, although still substantial, correlation with a zonal wind change of order 20 m s^{-1} in December for the last solar cycle. The above cautionary comments apply here as well, and, in addition, this relationship disappeared in other winter months, so averaging over the winter season would produce substantially lower results.

The 20 m s^{-1} variation is, coincidentally, of the same order of magnitude as occurs with $\pm 25\%$ UV (Table 4a). It is important to note that the model temperature response is actually more like the LvL observations when smaller UV and wind variations are involved. Why the smaller variations seem to be sufficient is discussed in the following section.

c. Explanation of response to varying UV forcing

1) WINDS AND WAVE PROPAGATION

The E–P flux variations for the extreme ($\pm 25\%$) and more realistic ($\pm 5\%$) UV experiments in the different phases of the QBO are given in Fig. 12. In the control run, wave energy propagates vertically out of the troposphere, refracting to lower latitudes south of 60°N and to higher latitudes north of 60°N . In the $\pm 25\%$ runs, zonal winds increase substantially in the extratropical stratosphere with increased UV (Fig. 10). The influence these winds have on the vertical propagation of Rossby waves is given by the refraction index formula shown in Eqs. (1) and (2).

The values for the differences between $[+25]$ and $[-25]$ of each of the terms involving the vertical gradient of the zonal wind, the full $\partial q/\partial y$ term, and the resulting refraction index are shown in Table 5a along with the change in the vertical E–P flux. Increasing the UV produces an increase in the zonal wind, an effect which increases with altitude in the stratosphere. Thus, the term involving the vertical gradient of the zonal wind increases (a positive refraction index effect) (column 3); however, the change with altitude diminishes above 1.5 mb, so the second derivative of the zonal wind variation with altitude changes sign at that level (column 4). $\partial q/\partial y$ also depends upon the second derivative of the zonal wind change with latitude, which is included in the calculation shown in column 5. The zonal wind increase itself acts to reduce the absolute value of the index, a result shown in column 6.

Overall, $\partial q/\partial y$ and the refraction index generally show a positive change above the middle stratosphere and a decrease below with UV increases of this magnitude, driven primarily by the change in the vertical

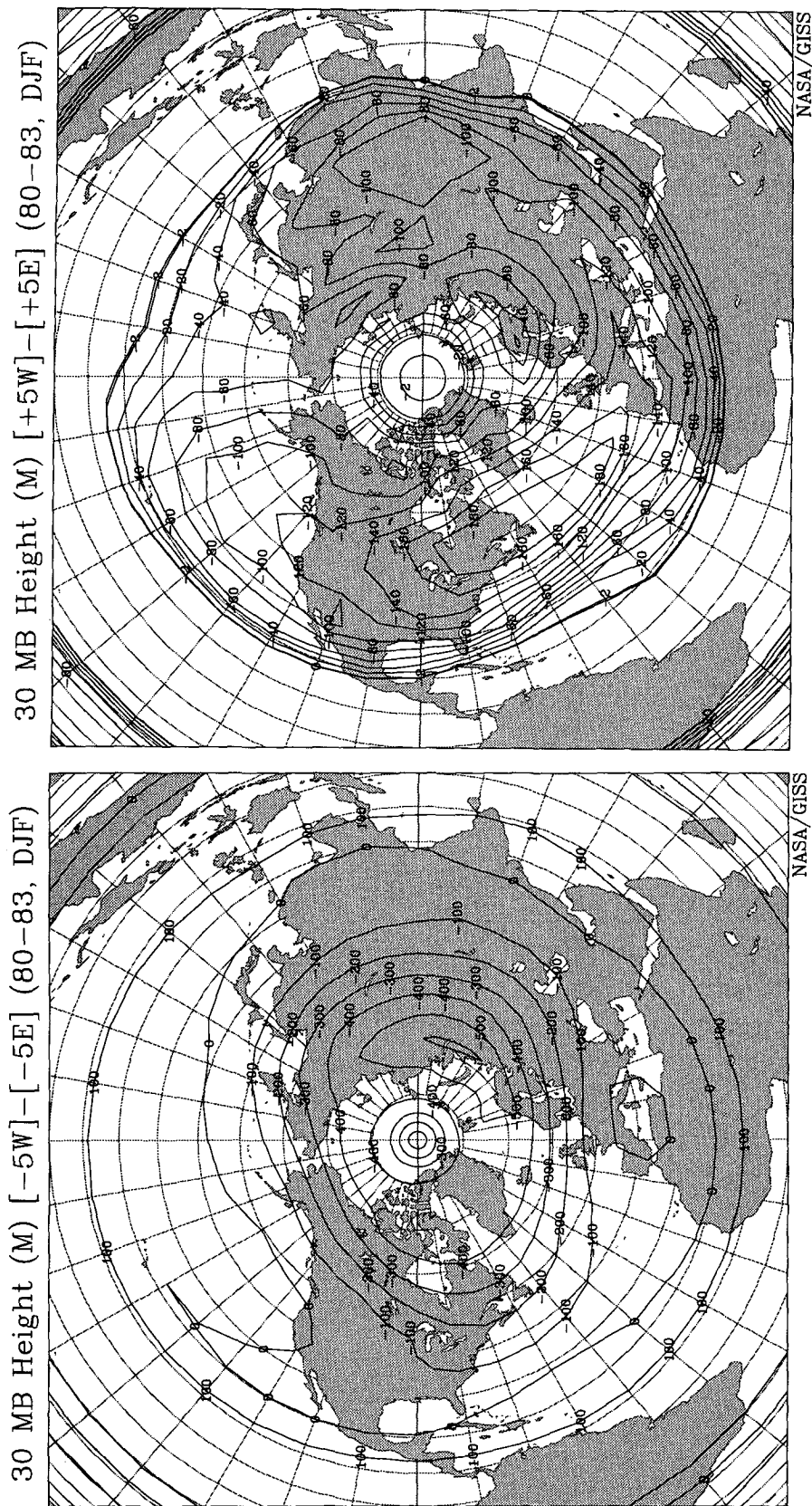


FIG. 7. Northern Hemisphere polar plots of geopotential height differences of 30-mb pressure surface (Dec-Feb averages) for (left) [-5W minus -5E] and (right) [+5W minus +5E].

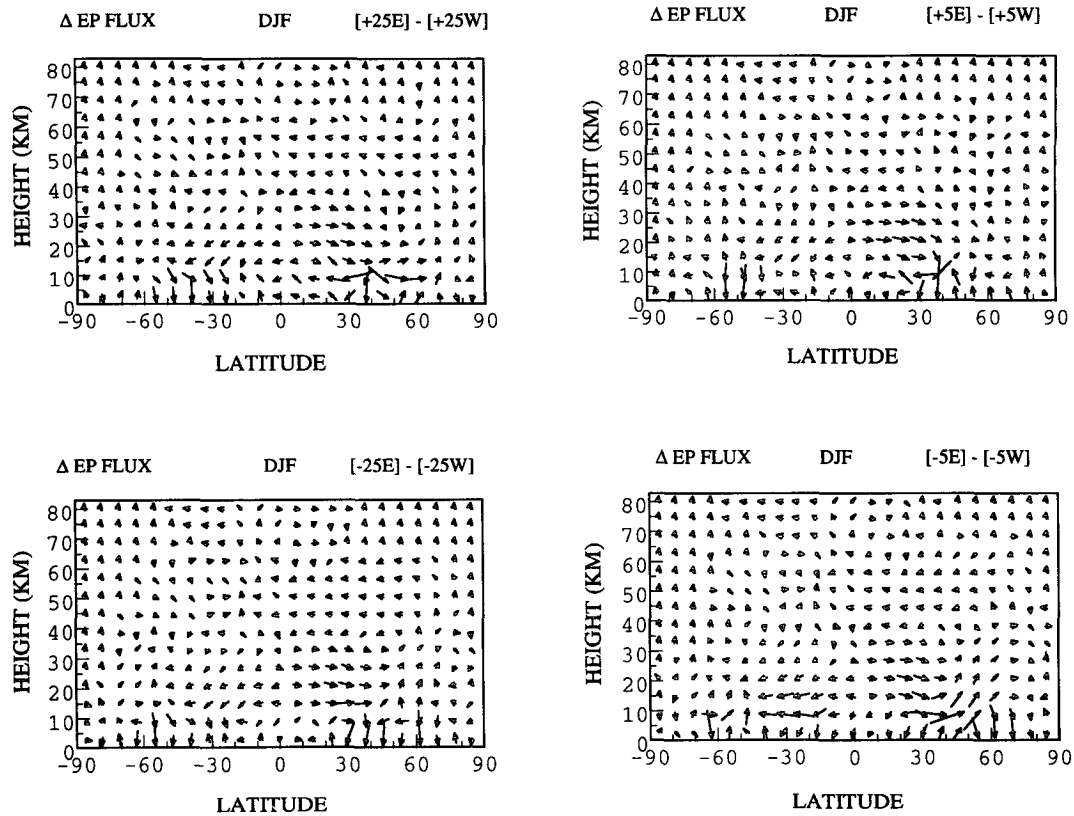


FIG. 8. E-P flux difference vectors in QBO experiments (Dec-Feb averages): [+25E minus +25W] (top left); [-25E minus -25W] (bottom left); [+5E minus +5W] (top right); [-5E minus -5W] (bottom right). The scale for the arrows that are discernible is $1'' = 8 \times 10^{18}$ J.

gradients. (Note: these calculations should be viewed as illustrative, since the quasigeostrophic refraction index is only of limited use in a primitive equation model.) The vertical E-P flux shows a similar tendency. Therefore, the 25% runs show an increased vertical propagation effect in conjunction with a more positive refraction tendency above the middle stratosphere with increased UV. (Note further that the refraction index formula assumes stationary waves, while the E-P flux values also include transient waves, so this comparison is only approximate; however, the change in total eddy energy is paralleled by the change in stationary eddy energy.)

The wind changes associated with the $\pm 10\%$ runs are also shown in Table 4a. In comparison with the

$\pm 25\%$ runs, the 10% changes have weaker wind increases (although the effect has not been reduced proportionately). The wave energy propagation and the refraction terms in the 10% runs are presented in Table 5b, along with the changes from the 25% experiments (in the last two columns). In this case, the refraction index change is now negative throughout the middle and upper stratosphere; hence wave energy propagation is discouraged and the increased flux from below does not propagate through 10 mb. In comparison with the more extreme (25%) UV variations, the first derivative of the vertical shear of the zonal wind is weaker due to the weaker radiative forcing, and both the upward energy propagation to higher levels and the refraction terms are more negative above the middle stratosphere.

TABLE 3. Change in Dec-Feb horizontal E-P flux and wave refraction properties for the different QBO experiments averaged from 30° to 67°N and 100 to 10 mb.

| | [E] minus [W] | [+25E] minus [+25W] | [-25E] minus [-25W] |
|---|---------------|---------------------|---------------------|
| Δ northward E-P flux (10^{16} J) | 56 | 48 | 88 |
| $\Delta \partial q / \partial y$ (10^{-11} s $^{-1}$ m $^{-1}$) | 18 | 20 | 12 |
| Δn^2 (10^{-7} m $^{-2}$) | 2.2 | 2.5 | 1.7 |

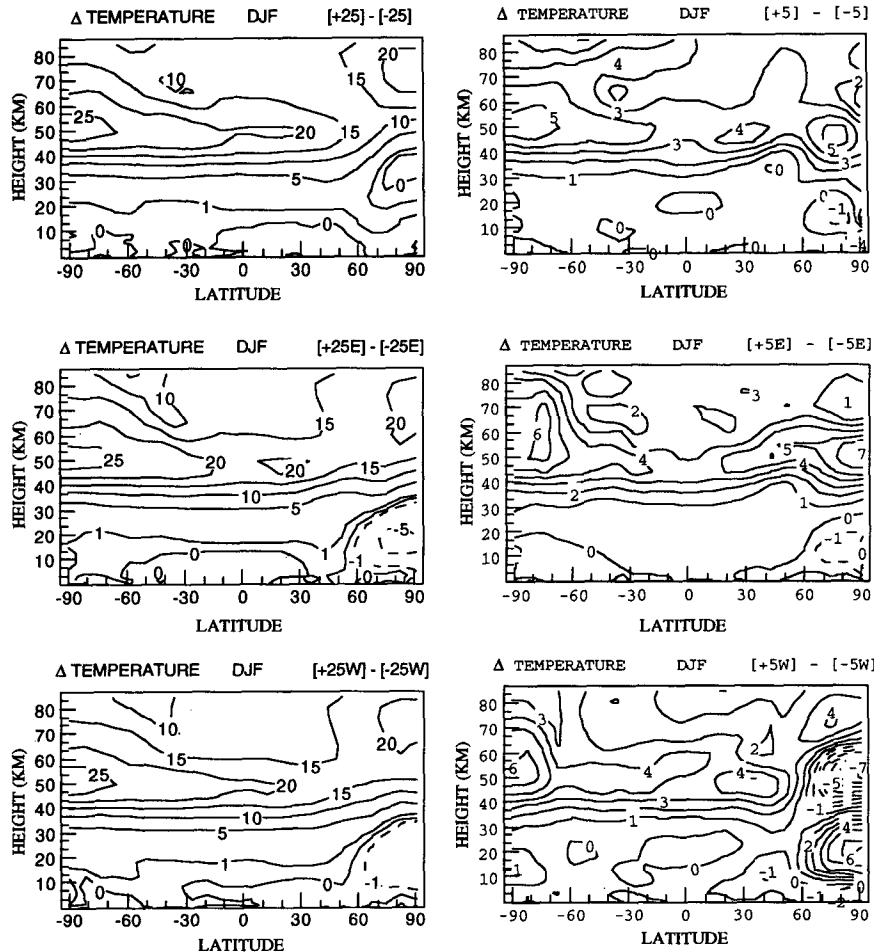


FIG. 9. Temperature differences for UV change experiments (Dec–Feb averages): [+25 minus –25] (top left); [+25E minus –25E] (middle left); [+25W minus –25W] (bottom left); [+5 minus –5] (top right); [+5E minus –5E] (middle right); [+5W minus –5W] (bottom right).

Thus, the 10% UV differences have increased propagation at lower levels and decreased propagation at upper levels when compared with the 25% UV variations. With the change in level of wave energy convergence, there are differences in altitude of the temperature response in these experiments (not shown).

The $\pm 5\%$ runs have a much smaller zonal wind change, with an effect that maximizes at lower altitudes (Table 4a; we first use the difference in the experiment without QBO forcing in an attempt to isolate the UV effect). The influence on the change in the refraction terms is given in Table 5c. Now the change in the second derivative of the wind velocity vertical shear favors propagation in the lower to midstratosphere. Of crucial importance here is the *profile* of the wind velocity change: Vertical propagation is favored where it increases with altitude (from the first derivative) and where this increase has a local maximum in altitude (from the second derivative). In addition, the horizontal gradient of

the zonal wind, in particular the second derivative, is also favoring increased propagation as the wind velocity change maximizes at upper midlatitudes (Fig. 10, top right). Although the wind velocity changes are not large, the vertical E–P flux appears to respond to more favorable propagation conditions whenever they are presented. It is also important to realize that the changes shown in Table 4a have already been affected by the changes in wave energy propagation and convergence and are not necessarily the radiative-induced wind velocity changes, as will be discussed further below.

The difference between the 5% and 25% experiments are shown in the last two columns of Table 5c. The 5% UV differences have more favorable propagation conditions in the lower stratosphere and greater vertical wave energy flux, differences of the same nature as occurred between the 25% and 10% runs (Table 5b). Above 10 mb, conditions have reversed as the weaker UV variations and weaker wind variations lead to re-

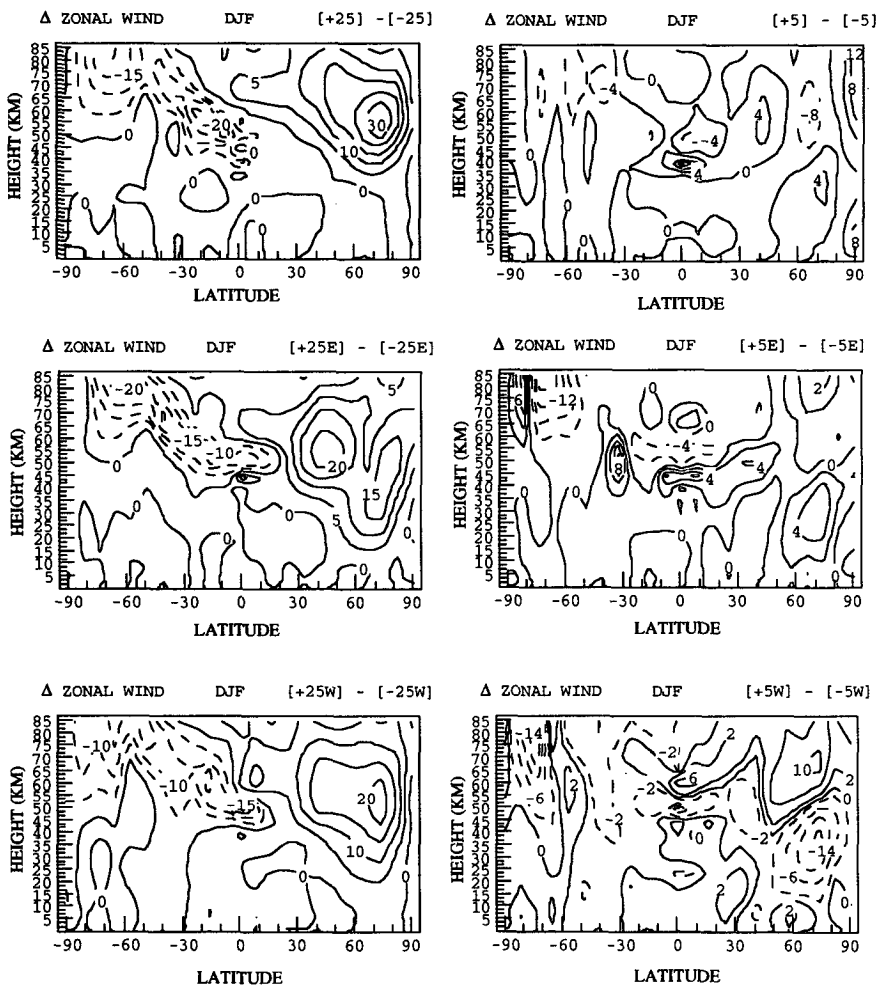


FIG. 10. As in Fig. 9 except for zonal wind differences in UV change experiments.

duced propagation and weaker vertical fluxes in the 5% runs.

2) RADIATIVE FORCING

The differences in wave propagation and associated effects in the lower and upper stratosphere are the result

of the changed wind profile arising with different magnitudes of UV forcing. It is therefore important to explore why the wind profiles are so different. As shown in Table 4a, the 5% results are at variance with what would be expected by a simple linear extrapolation

TABLE 4a. Zonal wind ($m s^{-1}$), 50° – 70° N, Dec–Feb.

| Pressure (mb) | Control | +25 | +10 | +5 | +5E | +5W |
|---------------|---------|-----------|-----------|----------|-----------|-----------|
| | | minus -25 | minus -10 | minus -5 | minus -5E | minus -5W |
| 0.316 | 71.5 | 23.4 | 14.2 | -4.2 | -0.7 | 5.3 |
| 0.68 | 64.6 | 20.0 | 11.7 | -3.7 | -0.3 | 0.1 |
| 1.5 | 50.3 | 14.2 | 8.2 | -2.2 | 1.0 | -5.2 |
| 3.2 | 35.3 | 8.3 | 4.8 | 0.2 | 2.6 | -9.1 |
| 6.8 | 24 | 3.3 | 2.3 | 2.4 | 3.9 | -10.7 |
| 14.7 | 17.7 | -0.4 | .8 | 3.3 | 4.4 | -10.1 |
| 31.6 | 16.3 | -2.3 | .2 | 3.1 | 4.4 | -7.8 |
| 68 | 17.4 | -2.8 | .5 | 2.1 | 4.0 | -4.3 |
| 149 | 19.3 | -2.1 | 1.2 | 1.2 | 2.8 | -0.7 |

TABLE 4b. Heating rate difference and zonal wind response between 43° and 74° N, Dec–Feb.

| Pressure (mb) | Control | Solar heating forcing ($^{\circ}C d^{-1}$) | | | Zonal wind response ($m s^{-1}$) | | |
|---------------|---------|--|---------------|-------------|------------------------------------|---------------|-------------|
| | | +25 minus -25 | +10 minus -10 | +5 minus -5 | +25 minus -25 | +10 minus -10 | +5 minus -5 |
| 0.316 | 5.51 | 2.32 | 0.72 | 0.46 | 154 | 53 | 30 |
| 0.68 | 8.26 | 3.70 | 1.26 | 0.74 | 116 | 41 | 23 |
| 1.5 | 6.56 | 2.43 | 0.91 | 0.49 | 54.5 | 20 | 11 |
| 3.2 | 3.3 | 0.60 | 0.23 | 0.12 | 12.5 | 4.7 | 2.5 |
| 6.8 | 1.93 | 0.91 | 0.03 | 0.02 | 1.7 | 0.6 | 0.4 |
| 14.7 | 1.06 | 0.01 | 0.00 | 0.00 | 0.1 | 0.0 | 0.0 |
| 31.6 | .57 | 0 | 0 | 0 | 0 | 0 | 0 |

TABLE 4c. Dynamical forcing (10^{-6} m s^{-2}) of the zonal wind by eddies and total, and zonal wind response (ms^{-1}), 50° – 70°N , Dec–Feb.

| Pressure (mb) | +25 | +10 | +5 | +25 | +10 | +5 | +25 | +10 | +5 |
|------------------|--|--|---|------------------------|------------------------|-----------------------|--------------------------------------|--------------------------------------|-------------------------------------|
| | minus 25 ($\nabla \cdot \mathbf{E}-P$) | minus 10 ($\nabla \cdot \mathbf{E}-P$) | minus 5 ($\nabla \cdot \mathbf{E}-P$) | minus 25 (Total) | minus 10 (Total) | minus 5 (Total) | minus 25 (m s^{-1}) | minus 10 (m s^{-1}) | minus 5 (m s^{-1}) |
| 0.316 | 10.7 | -2.1 | -36.6 | -1.8 | -2.5 | -0.7 | -4.7 | -6.5 | -1.8 |
| 0.68 | 40.4 | 3.4 | -18.9 | -0.4 | -1.7 | -1.5 | -1.0 | -4.4 | -3.9 |
| 1.5 | 41.4 | 8.1 | -7.0 | 1.5 | -0.1 | -2.1 | 3.9 | -0.3 | -5.4 |
| 3.2 | 32.7 | 13.4 | 0.9 | 3.0 | 0.5 | -2.6 | 7.8 | 1.3 | -6.7 |
| 6.8 | 17.3 | 12.9 | 13.5 | 3.3 | 0.8 | -2.2 | 8.6 | 2.1 | -5.7 |
| 14.7 | 0.4 | 6.4 | 14.8 | 2.7 | 0.8 | -1.4 | 7.0 | 2.1 | -3.6 |
| 31.6 | -5.9 | 0.6 | 8.3 | 1.7 | 0.9 | -0.6 | 4.4 | 2.3 | -1.6 |
| 68 | -7.7 | -1.5 | 0.3 | 1.1 | 0.8 | 0.1 | 2.9 | 2.1 | 0.3 |
| 149 | -9.2 | 1.4 | -4.4 | 0.5 | 0.8 | 0.7 | 1.3 | 2.1 | 1.8 |

from the larger UV variations. The change in UV radiation heating rate gradient still peaks in the upper stratosphere, but the west wind increase is now in the

middle stratosphere. Shown in Table 4b are the changes in solar radiation heating rates as a function of altitude between 43° and 74°N during winter for the different UV extremes, as calculated by the model. Comparing the upper stratosphere (1.5 mb) to the middle stratosphere (14.7 mb), the absolute value of the heating difference goes from $2.42^{\circ}\text{C d}^{-1}$ with $\pm 25\%$ to $0.49^{\circ}\text{C d}^{-1}$ with $\pm 5\%$, or a decrease of about a factor of 5 (consistent with the change in total UV variation). Hence, the radiational control favoring the upper-stratospheric response is weakened as the absolute value of the UV change decreases.

What effect would this radiation by itself have on the wind profile? We can make a crude estimate by calculating what the radiative temperature difference in response to this latitudinal heating gradient would be and relating the temperature change to zonal wind shear through the thermal wind relationship. Assuming no dynamical response, the temperature gradient will be a function of the incoming solar radiation change and the outgoing longwave radiative response. For the change in shortwave heating we use the values in Table 4b. For the outgoing response, we cannot use the model values since they have been affected by atmospheric dynamical changes. Therefore, we use a longwave radiative damping time constant for the appropriate altitudes. Andrews et al. (1987) show values ranging from less than 0.1 day^{-1} in the lower stratosphere to 0.2 day^{-1} in the lower mesosphere. When acting on the temperature perturbations driven by the shortwave heating, this then helps provide an estimate of the total radiative forcing.

Averaged over a month, the radiative forcing will generate temperature gradients between 43° and 74°N and, assuming hydrostatic and geostrophic equilibrium, will force the zonal wind response as a function of altitude, which is given in the last three columns of Table 4b. With the more extreme UV variations, very large vertical shears of the zonal wind result, a factor of 5 larger than with the more realistic UV forcing, again consistent with the UV change between the sets of experiments.

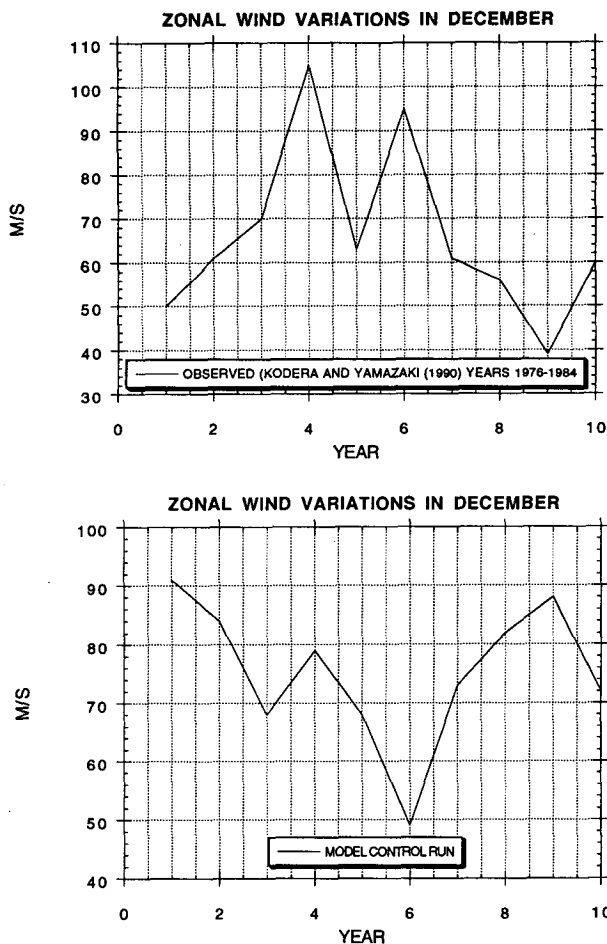


FIG. 11. Zonal wind variations in Dec at 1 mb. Observed variations (top) are for years 1976–1985 at 45°N (from Kodera and Yamazaki 1990); model variations (bottom) are from a 10-year simulation of the control run without UV or QBO variations at 60°N .

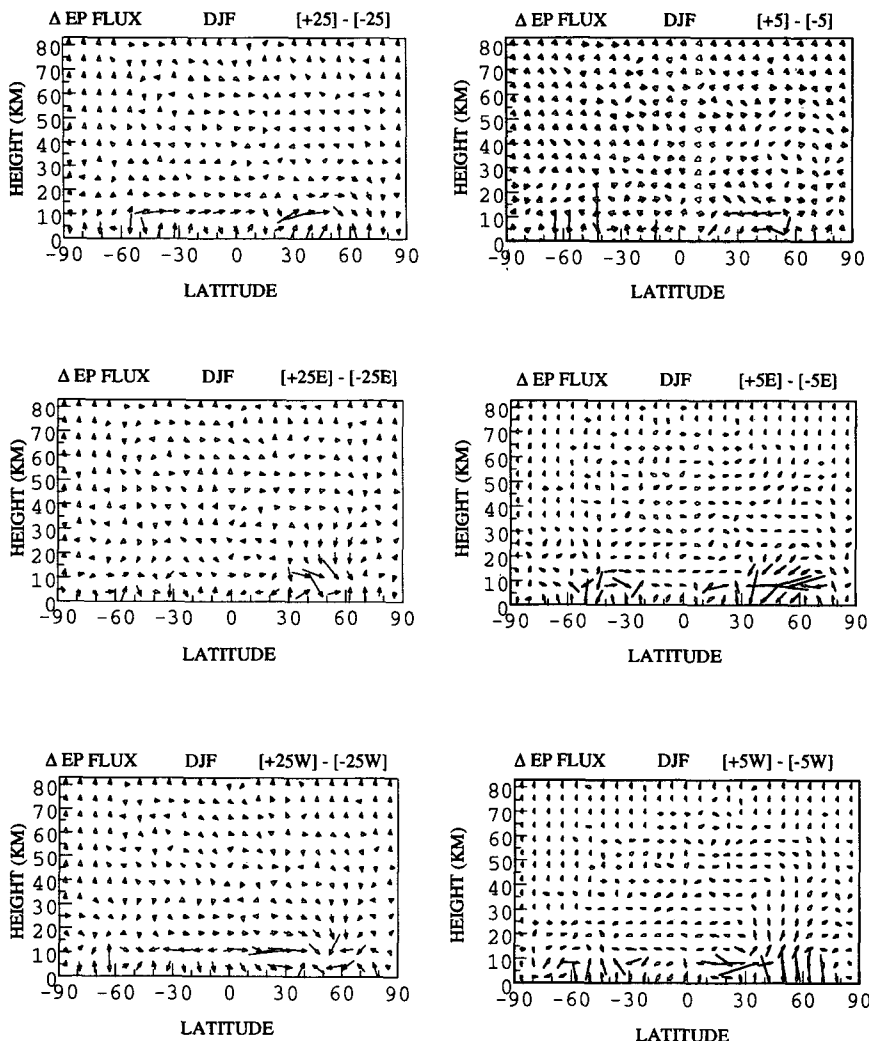


FIG. 12. As in Fig. 9 except for E-P flux differences in the UV change experiments. The scale for the arrows that are discernible is $1'' = 4 \times 10^{18}$ J.

While these winds are of course never realized, because of the dynamic response of the atmosphere (e.g., wave transports), they are the tendencies being forced by the UV variations. These wind tendencies then generate tendencies in propagation conditions. Shown in

Table 5d are the differences these “radiative winds” produce for the vertical gradients of the zonal wind in the refraction terms between the $\pm 5\%$ experiments and the $\pm 25\%$ experiments. The linear wind shear term is more negative throughout with the reduced UV vari-

TABLE 5a. Change in Dec-Feb vertical E-P flux and refraction index terms 50° - 70° N for +25 minus -25.

| Pressure (mb) | Vertical E-P flux (10^{14} J) | $H^{-1}(\partial U/\partial Z)$ ($10^{-8} \text{ m}^{-1} \text{ s}^{-1}$) | $-\partial^2 U/\partial Z^2$ ($10^{-8} \text{ m}^{-1} \text{ s}^{-1}$) | $\partial q/\partial y$ ($10^{-12} \text{ m}^{-1} \text{ s}^{-1}$) | n^2 (10^{-9} m^{-2}) |
|---------------|----------------------------------|---|--|--|------------------------------------|
| 0.464 | 40 | 8.5 | 20.0 | 10.9 | -1.3 |
| 1 | 96 | 14.5 | 5.0 | 6.8 | 0.7 |
| 2.2 | 132 | 14.8 | -1.6 | 2.0 | 1.4 |
| 4.6 | 174 | 12.5 | -6.0 | -2.2 | 0.6 |
| 10 | 42 | 7.3 | -6.0 | -5.3 | -0.8 |
| 21.5 | -454 | 4.8 | -4.0 | -6.4 | -4.1 |
| 46.4 | -1140 | 1.3 | -5.0 | -5.2 | -4.4 |

TABLE 5b. Change in Dec–Feb vertical E–P flux and refraction index terms 50°–70°N for +10 minus –10.

| Pressure (mb) | Vertical | $H^{-1}(\partial U/\partial Z)$ ($10^{-8} \text{ m}^{-1} \text{ s}^{-1}$) | $-\partial^2 U/\partial Z^2$ ($10^{-8} \text{ m}^{-1} \text{ s}^{-1}$) | $\partial q/\partial y$ ($10^{-12} \text{ m}^{-1} \text{ s}^{-1}$) | n^2 (10^{-9} m^{-2}) | Δ vertical E–P flux | | Δn^2 {+10–10} – {+25–25} |
|------------------|-------------------------------------|--|---|---|---------------------------------------|----------------------------|---------------------|-------------------------------------|
| | E–P flux (10^{14} J) | | | | | {+10–10} – {+25–25} | {+10–10} – {+25–25} | |
| 0.464 | –170 | 6.3 | 5.2 | 3.5 | –1.2 | –210 | 0.1 | |
| 1 | –354 | 8.8 | 1.8 | 1.7 | –0.7 | –450 | –1.4 | |
| 2.2 | –458 | 8.5 | –2.0 | –0.1 | –1.1 | –590 | –2.5 | |
| 4.6 | –393 | 6.3 | –3.8 | –1.5 | –3.1 | –567 | –3.7 | |
| 10 | –345 | 3.8 | –3.8 | –1.9 | –3.9 | –387 | –3.1 | |
| 21.5 | 383 | 1.5 | –3.6 | –1.4 | –2.1 | 837 | 2.0 | |
| 46.4 | 470 | –0.8 | –2.6 | –0.2 | 0.7 | 1610 | 3.7 | |

ations, while the second derivative term is more negative at high levels and more positive at low levels due to the greater change with altitude of the linear wind shear, which maximizes in both cases at 1.5 mb. Overall, the propagation conditions are more favorable with the greater UV variations in the upper stratosphere/lower mesosphere, while they are more favorable with reduced UV variations in the low to middle stratosphere. Note this result largely mimics the differences that result from the actual wind changes in the 5% and 25% experiments (right-hand columns of Table 5c).

3) DYNAMICAL FORCING

In conjunction with this radiative influence, there is a change in the dynamical forcing of the zonal wind. The direct eddy forcing (associated with the divergence of the E–P flux) is indicated in Table 4c for the different UV experiments. Also shown are the total change in zonal wind forcing, the sum of alterations in the E–P flux divergence, transformed circulation advection, gravity wave drag, and diffusion. The transformed (residual) circulation is itself forced by eddies, as well as by diabatic heating.

Considering first the direct eddy forcing, as the UV variations become less extreme, the region of positive eddy forcing (E–P flux divergence) decreases in altitude. This is in qualitative approximate agreement with the tendencies associated with the radiative forcing (Table 5d): the energy propagation in the more extreme UV experiments is favored at higher levels relative to lower levels, providing for E–P flux divergences in the upper stratosphere–lower mesosphere, while with reduced UV, the propagation is favored at lower levels, hence generating E–P flux divergences in the lower and middle stratosphere. The $\pm 10\%$ experiments produce intermediate effects in altitude.

The total dynamical forcing (Table 4c) indicates that increased UV in the 25% experiments is accelerating the wind in the upper stratosphere, while increased UV in the 5% runs is decelerating the winds there. When averaged over a month, the wind changes due to the total forcing for the respective experiments are shown in the final three columns. The differences among the dynamical forcings help explain why the wind changes

in the 5% experiments are not simple linear extrapolations from the more extreme UV experiments, and in particular, why the 5% changes are so small in the upper stratosphere (Table 4a). The maximum zonal wind change in those runs occurs in the middle stratosphere. Despite the positive eddy forcing at those levels during winter, the total forcing is still decelerating the winds there due to the mountain wave drag (the eddy plus transformed advection effect is positive). However, in the other nine months of the year the total forcing is positive in the middle stratosphere as the mountain drag is smaller; hence the deceleration during winter still leaves positive zonal wind changes peaking at 14.7 mb. The process of course is highly interactive, for the peak in the middle stratosphere allows the second derivative of the zonal wind variation with altitude to provide a positive influence on wave energy propagation through that region.

The differences in wave energy fluxes between the 25% runs and between the 5% runs, respectively, can be seen in Fig. 12 (top); the wave energy flux changes in the Northern Hemisphere extratropics are of opposite direction throughout the middle atmosphere (and in the troposphere as well). Ultimately, the difference is driven by the change in vertical gradient of heating, but it is altered by the response of wave energy propagation itself.

6. QBO/UV results

The results depicted in Tables 4 and 5 apply to the UV variations without influence from the QBO. As can be seen in Table 2 and Figs. 9, 10, and 12, conditions are affected by the presence of the QBO, especially for the 5% experiments. Table 4a also shows the zonal wind variations in the two QBO phases for the 5% experiments. In the east phase, the results are fairly similar to those without any explicit QBO; the control run values show light east winds at the equator without any forcing (Fig. 1). However, in the west phase, zonal winds have decreased throughout the middle stratosphere. The QBO alters wave energy propagation by varying the horizontal shear of the zonal wind in the lower stratosphere, while UV variations in the model have an effect on wave propagation by al-

TABLE 5c. Change in Dec–Feb vertical E–P flux and refraction index terms 50°–70°N for +5 minus –5.

| Pressure | Vertical E–P flux (10 ¹⁴ J) | $H^{-1}(\partial U/\partial Z)$ (10 ⁻⁸ m ⁻¹ s ⁻¹) | $-\partial^2 U/\partial Z^2$ (10 ⁻⁸ m ⁻¹ s ⁻¹) | $\partial q/\partial y$ (10 ⁻¹² m ⁻¹ s ⁻¹) | n^2 (10 ⁻⁹ m ⁻²) | Δ vertical E–P flux {+5–5} minus {+25–25} | Δn^2 {+5–5} minus {+25–25} |
|----------|--|---|--|--|---|--|------------------------------------|
| 0.464 | 28 | -1.3 | -2.8 | -3.6 | -0.5 | -24 | 0.8 |
| 1 | 24 | -3.6 | -2.9 | -1.2 | 0.1 | -86 | -0.6 |
| 2.2 | 24 | -5 | -1.5 | 7.6 | 0.4 | -124 | -1.0 |
| 4.6 | 123 | -5.6 | 2.2 | 6.2 | 1.8 | -36 | 1.2 |
| 10 | 383 | -2.3 | 5.0 | 7.4 | 5.3 | 304 | 6.1 |
| 21.5 | 520 | .7 | 3.7 | 5.8 | 4.0 | 792 | 8.1 |
| 46.4 | 172 | 2.3 | 1.3 | 3.0 | -0.8 | 178 | 3.6 |

tering the vertical shear of the zonal wind in the stratosphere. How do the results of these two phenomena interact?

During the east phase of the QBO, wave energy propagates preferentially to the pole in the lower stratosphere; however, whether this energy actually converges there depends upon whether it propagates vertically or not. With increased UV, vertical propagation is favored, hence less of the wave energy converges in the lower stratosphere, and the polar heating is reduced (Fig. 5). In the 25% runs, the largest difference in wave energy propagation occurs above the midstratosphere (Table 5a), for it is at those altitudes where the large wind increases occur. In the 5% runs, the largest difference is in the lower stratosphere, and since this is the region directly affected by the QBO, the 5% UV variations maximize their effect on the QBO (Fig. 5).

The results can also be viewed from the framework of the UV impacts during differing phases of the QBO (Fig. 9). During the east phase, the UV maximum produces cooling in the polar lower stratosphere, while during the west phase it produces warming with 5% UV changes. The resulting wind velocity changes are therefore also much different (Table 4a, Fig. 10), with increased zonal winds through the extratropical stratosphere during the UV maximum in the east phase and decreased zonal winds in the 5% experiments during the west phase.

As a consequence of this change in wind pattern, wave refraction patterns are different. As indicated in

Fig. 12, the 5% runs have almost an opposite wave refraction change in the east and west phases. The effect of the differing zonal winds on propagation is explored in Table 6. The increased high-latitude zonal winds during the east phase lead to increased vertical propagation at the highest latitudes; hence there is relative wave energy divergence, the zonal winds are stronger, and the lower stratosphere is cooler. This of course is the equilibrium situation, which must therefore be self-consistent, and it follows from the combined influence of changes in the horizontal shear from the QBO and the vertical shear from the altered UV. The effect is stronger in the 5% runs because the lower levels in the stratosphere are being affected.

7. Consistency of results and statistical significance

The experiments described above were run for just three years, and while the model diagnostics indicate the physical processes responsible for the results, they may, as also suggested by one of the reviewers, be associated with the model's natural variability rather than the imposed forcing. To investigate this possibility, all the 5% experiments were extended to 10 years. The most intriguing conclusions from the 3-year runs are epitomized by the differences in temperature response between the E and W runs for the +5% UV change and the –5% UV change, respectively (Fig. 5, right), and the difference between the +5% and –5% runs for the E phase and W phase, respectively (Fig. 9, right). In Fig. 13 we show the results of the 10-year averages for these experiments. Comparing Figs. 5 and 9, it can be seen that the similarities are remarkable in both the overall pattern and magnitude of the temperature response. Other aspects of the results are similar as well. For the 10-year run, assuming each year is independent, the larger temperature variations are now statistically significant at the 95% level. It is fair to conclude that the response seen in these experiments, whether on the 3- or 10-year averages, are due to the imposed forcing and are robust.

8. Discussion and conclusions

The GCM does not produce a QBO directly; however, when QBO forcing is introduced, the model re-

TABLE 5d. Change in Dec–Feb refraction index terms (units 10⁻⁸ m⁻¹ s⁻¹), 50°–70°N for the radiative driven winds of Table 4b, (+5 minus –5) minus (+25 minus –25).

| Pressure | $H^{-1}(\partial U/\partial Z)$ | $-\partial^2 U/\partial Z^2$ | $\Sigma(2-3)$ |
|----------|---------------------------------|------------------------------|---------------|
| 0.316 | -57.5 | -56 | -114 |
| 0.68 | -100 | -74 | -174 |
| 1.5 | -104 | 64 | -40 |
| 3.2 | -64.3 | 100 | 35.7 |
| 6.8 | -15.1 | 30.2 | 15.1 |
| 14.8 | -1.9 | 4.4 | 2.5 |
| 31.6 | -0.1 | 0.4 | 0.3 |

lations of the Mg index solar activity proxy with the short-term (27 days) UV irradiance rotational modulation measured by the Solar Stellar Irradiance Comparison Experiment (SOLSTICE) on the *Upper Atmosphere Research Satellite* (Rottman et al. 1993). The dashed line shows the variability measured directly in solar cycle 21 by the Solar Mesosphere Explorer (SME) (Rottman 1988). Variations of 4%–8% occur from 200 to 250 nm, with generally decreasing values to 300 nm. In addition, preliminary evaluation of long-term variations measured in solar cycle 22 by the *UARS* also indicate solar cycle variations of the order of 8% near 200 nm and up to 6% in the region 210–250 nm. In comparison, the UV forcing used in the most realistic experiments (the $\pm 5\%$ variations) amount to 10% throughout the spectrum short of 300 nm. The ability of the UV forcing to affect wave energy propagation, and the altitude of its major impact, depends upon the profile of the resulting wind variations, which in the model responds sensitively to the magnitudes of UV variations employed. It is perfectly conceivable that if the smaller UV variations appropriate to an actual solar cycle (Fig. 14) were used, the model's response could be different or negligible, although the model's results do actually look more like the observations with the more realistic 5% UV forcing. Apparently, an accurate prescription of the UV forcing along with any ozone changes will be needed for judging the true impact of solar UV/QBO coupling.

Second, observations imply a strong wind variation in the upper stratosphere that has been associated with the (last) solar cycle (Kodera and Yamazaki 1990). Even the smaller variations deduced by Hood et al. (1993) can only be reproduced in the model with UV variations that are much more extreme than is observed. If such wind variations are required for lower-atmospheric effects, as suggested by one of the reviewers, these model experiments cannot associate them with realistic solar UV forcing. The model can simulate the strong wind variations seen in the data in its control run *without* altered solar UV forcing (Fig. 11), raising the possibility that natural variability is responsible for the observations. Ironically, it is the *smaller* wind variations associated with more realistic UV forcing that produce the best results when coupled with the QBO. In fact, our results (Figs. 9 and 10) show that the lower-atmospheric temperature changes are associated with wind changes by dynamics in the lower stratosphere. What we have been able to show in these experiments is that with the crude UV variations employed in the model, the results suggest mechanisms involving wave dynamics that affect the lower stratosphere, although the UV changes mainly affect the upper stratosphere and the energy involved is small.

In this paper we have concentrated on the impacts above the tropopause. Some of the influences appear to extend into the troposphere; these will be explored in Part II. We note that while we have exaggerated the

UV changes in these experiments, we have underestimated the visible and IR changes accompanying the solar cycle. These latter alterations could presumably have an impact in the troposphere. A full assessment of the atmospheric response to the solar cycle will have to include a proper prescription of changes at all wavelengths.

Acknowledgments. We thank Patrick Lonergan for his help in setting up model experiments and providing diagnostic output of the results. Alan Plumb helped design the QBO experiments and some model diagnostics and offered suggestions on the manuscript. Ron Nagatani kindly provided NMC observations for comparison with model results. Judith Lean provided advice concerning solar UV variations and provided Fig. 14. This work was supported by NSF Solar Terrestrial Physics Grant ATM9208266, while the model development work has been funded by the NASA Upper Atmosphere Program Office.

REFERENCES

- Andrews, D. G., J. R. Holton, and C. B. Leovy, 1987: *Middle Atmosphere Dynamics*. Academic Press, 489 pp.
- Balachandran, N. K., R. A. Plumb, R. Suozzo, and D. Rind, 1991: The QBO and stratospheric warming-model results. *J. Geomagn. Geoelectr.*, **43**(Suppl.), 741–757.
- Barnston, A. G., and R. E. Livezey, 1989: A closer look at the effect of the 11-year solar cycle and the quasi-biennial oscillation on the Northern Hemisphere 700 mb height and extratropical North American surface temperature. *J. Climate*, **2**, 1295–1313.
- Dameris, M., and A. Ebel, 1990: The quasi-biennial oscillation and major stratospheric warmings: A three-dimensional model study. *Ann. Geophysicae*, **8**, 79–86.
- Dunkerton, T. J., and M. P. Baldwin, 1991: Quasi-biennial modulation of planetary-wave fluxes in the Northern Hemisphere winter. *J. Atmos. Sci.*, **48**, 1043–1061.
- , and —, 1992: Modes of interannual variability in the stratosphere. *Geophys. Res. Lett.*, **19**, 49–52.
- , D. P. Delisi, and M. P. Baldwin, 1988: Distribution of major stratospheric warmings in relation to the quasi-biennial oscillation. *Geophys. Res. Lett.*, **15**, 136–139.
- Hansen, J. E., G. Russell, D. Rind, P. Stone, A. Lacis, S. Lebedeff, R. Ruedy, and L. Travis, 1983: Efficient three-dimensional global models for climate studies: Models I and II. *Mon. Wea. Rev.*, **111**, 609–662.
- Holton, J. R., and H.-C. Tan, 1980: The influence of the equatorial quasi-biennial oscillation on the global circulation at 50 mb. *J. Atmos. Sci.*, **37**, 2200–2208.
- , and —, 1982: The quasi-biennial oscillation in the northern hemisphere lower stratosphere. *J. Meteor. Soc. Japan*, **60**, 140–147.
- Hood, L. L., J. L. Jirikowic, and J. P. McCormack, 1993: Quasi-decadal variability of the stratosphere: Influence of long-term solar ultraviolet variations. *J. Atmos. Sci.*, **50**, 3941–3958.
- Huang, T. Y. W., and G. Brasseur, 1993: Effect of long-term solar variability in a two-dimensional interactive model of the middle atmosphere. *J. Geophys. Res.*, **98**, 20 413–20 427.
- Kodera, K., 1991: The solar and equatorial QBO influences on the stratospheric circulation during the early Northern Hemisphere winter. *Geophys. Res. Lett.*, **18**, 1023–1026.
- , 1993: Quasi-decadal modulation of the influence of the equatorial quasi-biennial oscillation on the north polar stratosphere temperatures. *J. Geophys. Res.*, **98**, 7245–7250.

- , and K. Yamazaki, 1990: Long-term variation of upper stratospheric circulation in the Northern Hemisphere in December. *J. Meteor. Soc. Japan*, **68**, 101–105.
- , K. Yamazaki, M. Chiba, and K. Shibata, 1990: Downward propagation of upper stratospheric mean zonal wind perturbation to the troposphere. *Geophys. Res. Lett.*, **17**, 1263–1266.
- Labitzke, K., 1982: On the interannual variability of the middle stratosphere during northern winters. *J. Meteor. Soc. Japan*, **60**, 124–139.
- , 1987: Sunspots, the QBO, and the stratospheric temperature in the north polar region. *Geophys. Res. Lett.*, **14**, 135–137.
- , and H. van Loon, 1992: On the association between the QBO and the extratropical stratosphere. *J. Atmos. Terr. Phys.*, **54**, 1453–1463.
- Lean, J., 1991: Variations in the sun's radiative output. *Rev. Geophys.*, **29**, 505–536.
- , M. VanHoosier, G. Brueckner, D. Prinz, L. Floyd, and K. Edlow, 1992: SUSIM/UARS observations of the 120 to 300 nm flux variations during the maximum of the solar cycle: Inferences for the 11-year cycle. *Geophys. Res. Lett.*, **19**, 2203–2206.
- O'Sullivan, D., and T. J. Dunkerton, 1994: Seasonal development of the extratropical QBO in a numerical model of the middle atmosphere. *J. Atmos. Sci.*, **51**, 3706–3721.
- Plumb, R. A., 1984: The quasi-biennial oscillation. *Dynamics of the Middle Atmosphere*, J. R. Holton and T. Matsuno, Eds., Terra Scientific Publishing, 217–251.
- Rind, D., R. Suozzo, N. K. Balachandran, A. Lacis, and G. Russell, 1988a: The GISS global climate/middle atmosphere model. Part I: Model structure and climatology. *J. Atmos. Sci.*, **45**, 329–370.
- , —, and —, 1988b: The GISS global climate–middle atmosphere model. Part II: Model variability due to interactions between planetary waves, the mean circulation and gravity wave drag. *J. Atmos. Sci.*, **45**, 371–386.
- Rottman, G. J., 1988: Observations of solar UV and EUV variability. *Adv. Space Res.*, **8**, 53–66.
- , T. N. Woods, and T. P. Sparn, 1993: Solar-Stellar Irradiance Comparison Experiment, 1, Instrument design and operation. *J. Geophys. Res.*, **98**, 10 667–10 677.
- Salby, M. L., and D. J. Shea, 1991: Correlations between solar activity and the atmosphere: An unphysical explanation. *J. Geophys. Res.*, **96**, 22 579–22 595.
- van Loon, H., and K. Labitzke, 1987: The Southern Oscillation. Part V: The anomalies in the lower stratosphere of the Northern Hemisphere in winter and a comparison with the Quasi-Biennial Oscillation. *Mon. Wea. Rev.*, **115**, 357–369.
- , and —, 1988: Association between the 11-year solar cycle, the QBO, and the atmosphere. Part II: Surface and 700 mb in the Northern Hemisphere winter. *J. Climate*, **1**, 905–920.